Your thesaurus codes are:
03(03.13.6),08(08.05.03),11(11.13.1; 11.04.1)

ASTROPHYSICS
March 22, 2000

The Tip of the Red Giant Branch and Distance of the Magellanic Clouds

Maria-Rosa. L. Cioni[1], **Roeland P. van der Marel**[2], **Cecile Loup**[3], **and Harm J. Habing**[1]

[1] Sterrewacht Leiden, Postbus 9513, 2300 RA Leiden, The Netherlands
[2] Space Telescope Science Institute, 3700 San Martin Drive, Baltimore, MD 21218, USA
[3] Institute d'Astrophysique de Paris, CNRS, 98 bis Bd. Arago, 75014 Paris, France

Abstract. We present a precise determination of the apparent magnitude of the tip of the red giant branch (TRGB) in the I (0.8μm), J (1.25μm), and K_S (2.15μm) bands from the luminosity function of a sample of data extracted from the DENIS catalogue towards the Magellanic Clouds (Cioni et al. 2000a). From the J and K_S magnitudes we derive bolometric magnitudes m_{bol}. We present a new algorithm for the determination of the TRGB magnitude, which we describe in detail and test extensively using Monte-Carlo simulations. We note that any method that searches for a peak in the first derivative (used by most authors) or the second derivative (used by us) of the observed luminosity function does not yield an unbiased estimate for the actual magnitude of the TRGB discontinuity. We stress the importance of correcting for this bias, which is not generally done. We combine the results of our algorithm with theoretical predictions to derive the distance modulus of the Magellanic Clouds. We obtain $m - M = 18.55 \pm 0.04$ (formal) ± 0.08 (systematic) for the Large Magellanic Cloud (LMC), and $m - M = 18.99 \pm 0.03$ (formal) ± 0.08 (systematic) for the Small Magellanic Cloud (SMC). These are among the most accurate determinations of these quantities currently available, which is a direct consequence of the large size of our sample and the insensitivity of near infrared observations to dust extinction.

Key words: Methods: statistical – Stars: evolution – Galaxies: Magellanic Clouds – Galaxies: distances

1. Introduction

In the evolution of stars the position of the tip of the red giant branch (TRGB) marks the starting point of helium burning in the core. It is one of the strongest characteristics of the life of stars seen in theoretical models, together with the main sequence turn–off point, the red giant and the asymptotic giant clump. It has been used successfully for several decades (Sandage 1971) to estimate the distance of resolved galaxies (e.g., Lee, Freedman & Madore 1993). The TRGB magnitude depends only very weakly on age and metallicity, and yields comparable precision as classical distance indicators such as Cepheids and RR–Lyra variables.

Cioni et al. (2000a) prepared the DENIS Catalogue towards the Magellanic Clouds (DCMC), as part of the Deep Near Infrared Southern Sky Survey performed with the 1m ESO telescope (Epchtein et al. 1997). The catalogue contains about 1 300 000 and 300 000 sources toward the LMC and the SMC, respectively; 70% of them are real members of the Clouds and consist mainly of red giant branch (RGB) stars and asymptotic giant branch (AGB) stars, and 30% are galactic foreground objects. This is a very large and homogeneous statistical sample that allows a highly accurate determination of the TRGB magnitude at the corresponding wavelengths. Among other things, this yields an important new determination of the distance modulus of the LMC. This distance modulus is one of the main stepping stones in the cosmological distance ladder, yet has remained somewhat uncertain and controversial (e.g., Mould et al. 2000).

Section 2 describes how the data were selected from the DCMC catalogue to avoid crowding effects, and how we have calculated bolometric corrections. Section 3 discusses the luminosity function (LF) and the subtraction of the foreground component. Section 4 discusses the TRGB determination and gives comparisons with previous measurements. Section 5 discusses the implications for the distances to the Magellanic Clouds. Concluding remarks are given in Section 6. The Appendix provides a detailed description of the new method that we have used to quantify the TRGB magnitude, as well a discussion of the formal and systematic errors in the analysis.

2. The Sample

2.1. The Data

The DCMC covers a surface area of 19.87 × 16 square degrees centered on $(\alpha, \delta) = (5^h27^m20^s, -69°00'00'')$ toward the LMC and 14.7 × 10 square degrees centered on

Send offprint requests to: mrcioni@strw.leidenuniv.nl

$(\alpha, \delta) = (1^h02^m40^s, -73°00'00'')$ toward the SMC (J2000 coordinates). We extracted all the sources detected simultaneously in the three DENIS photometric wave bands: I (0.8μm), J (1.25μm) and K_S (2.15μm). We excluded sources that were detected in all three wave bands but at different times (this can happen because DENIS strips overlap). The selection of sources that are present in all three wave bands strongly reduces possible crowding effects that affect mostly the I band. We removed sources affected, even slightly, by image defects (null image flag) and sources with bright neighbours or bad pixels, sources that were originally blended, or sources with at least one saturated pixel (null extraction flag). This increases the level of confidence on the resulting sample. The main final sample for the present analysis contains 33 117 sources toward the SMC and 118 234 sources toward the LMC. This constitutes about 10% of all the sources listed for each Cloud in the DCMC.

To estimate the contribution of the foreground component we also considered the data in offset fields outside the spatial limits of the DCMC[1], covering the same range in right ascension and from a maximum of $\delta = -57°$ to a minimum of $\delta = -87°$ (the full declination range of a DENIS strip). These data were reduced together and the same selection criteria, on the basis of the detection wave bands and the flags, were applied as to the data constituting the DCMC. The total sample (DCMC plus extension in declination) contains 92 162 and 184 129 sources in the RA ranges for the SMC and the LMC, respectively.

The distribution of the formal photometric errors in each wave band is shown in Fig. 1. At the brighter magnitudes (those of interest for the TRGB determination), the random errors in the sample are not dominated by the formal photometric errors, but by random errors in the photometric zero–points for the individual strips. The dispersions (1σ) of these zero-point variations are 0.07 mag in the I band, 0.13 mag in the J band and 0.16 mag in the K_S band. Note that the formal error with which the TRGB magnitude can be determined is not limited to the size of these zero-point variations, but instead can be quite small (the formal error is proportional to $1/\sqrt{N}$, where N is the number of stars in the sample).

The I, J and K_S magnitudes in the present paper are all in the photometric system associated with the DENIS passbands. These magnitudes are not identical to the classical Cousin I and CTIO J and K magnitudes, although they are close (differences are ≤ 0.1 magnitudes). The final transformation equations for the passbands will not be available until the survey is completed, but a preliminary analysis is presented by Fouqué et al. (1999). Note that our determinations of the distance moduli for the LMC and the SMC (Section 5) are based on bolometric magnitudes derived from the data, which are fully corrected for the specifics of the DENIS passbands.

[1] These data are not part of the DCMC catalogue but are available on request from the first author.

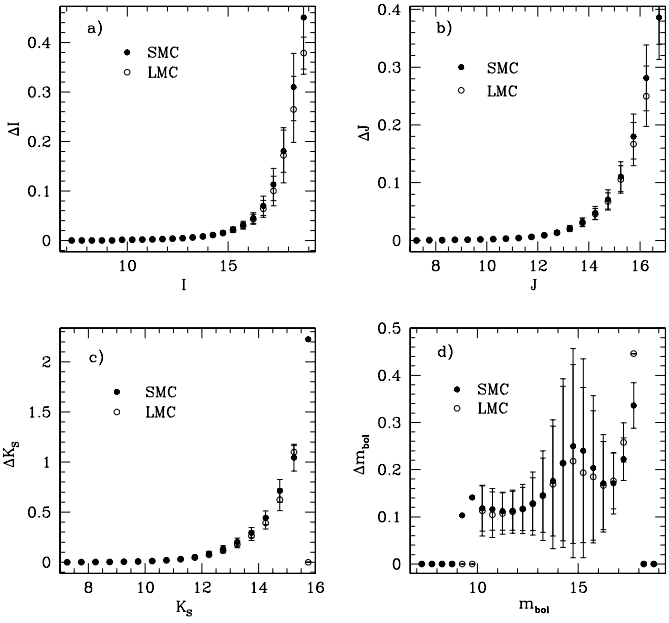

Fig. 1. Distribution of the photometric errors. (a) I band, (b) J band, (c) K_S band, (d) m_{bol}. Black dots are for sources toward the LMC and empty dots are for sources toward the SMC. Error bars show the dispersion in the photometric errors in 0.5 mag bins.

2.2. Bolometric correction

We have calculated the apparent bolometric magnitude (m_{bol}) for all the sources selected according to the criteria described in Section 2.1, and with $(J - K_S) \geq 0.4$. We have chosen to use only the J and K_S bands to derive m_{bol} (see below). Sources with $(J - K_S) < 0.4$ do not influence the position of the TRGB (see Fig. 5 below), and have too low a percentage of flux in the near-infrared (NIR) to give a reliable measure of m_{bol} with these criteria. We used two different bolometric corrections, depending on the $(J - K_S)$ colour. For sources with $(J - K_S) < 1.25$, we simply use a blackbody fit on the $(J-K_S)$ colour; such sources are mostly RGB or early AGB (E–AGB) stars in our sample. Sources with larger values of $(J - K_S)$ are mostly thermal pulsing AGB (TP–AGB) stars, some of which are losing mass and are surrounded by a circumstellar envelope. For them we used the results of individual modelling of galactic carbon (C) stars by Groenewegen et al. (1999), combined with a series of models of increasing dust opacity where the central star has a spectral type $M5$ and the dust grains are composed of silicates (Groenewegen, private communication).

In both cases, blackbody fit or spectral models, our method to infer m_{bol} is different from what is usually performed in the literature. We do not make any attempt to transform a magnitude, i.e. an integrated flux over the

passband, into a flux density at a reference wavelength, in order to suppress one step which already makes an assumption on the spectral distribution of the source. We only use the integrated flux measured over the J and K_S DENIS passbands. Theoretical spectral distributions, i.e. blackbodies with temperatures ranging from 10,000 to 300 K and the models from Groenewegen and collaborators, were multiplied with the DENIS passbands (which includes a mean atmosphere at la Silla observatory) to derive the percentage of the total flux which is measured in each DENIS passband as a function of the DENIS colours. Then, for each selected DCMC source, m_{bol} is calculated by interpolating in the theoretical grids the percentage of flux measured in the J and K_S bands from the observed $(J-K_S)$ colour. We have used here the same zero point as in Montegriffo et al. (1998). More details are provided in Loup et al. (2000).

We have compared our results with the bolometric corrections BC_K inferred by Montegriffo et al. As can be seen in their Fig. 3, their bolometric correction is valid only for sources with $0.2 < (J-K_S) < 0.7$, with a typical spread around the fit of 0.1 magnitude. For sources with $0.4 < (J-K_S) < 0.5$ our blackbody fit agrees with their bolometric corrections to within the errors. On the other hand, for some sources with $(J-K_S) > 0.5$, they underestimate m_{bol} by 0.5 to 2 magnitudes compared to our calculations. This is not surprising and can be inferred already from their Fig. 3; it does not indicate a shortcoming in our approach. We also compared our results with what one obtains by making blackbody fits using both the $(I-J)$ and $(J-K_S)$ colours. For sources with $0.4 < (J-K_S) < 1.25$ it does not produce any systematic effect; there is merely a spread of typically 0.1 magnitude between both calculations, consistent with the formal errors. Inclusion of the I band would produce a systematic effect for bluer sources than those selected here, but those are not relevant for the TRGB determination. We therefore decided to use only the J and K_S band data in our calculations of $m_{\rm bol}$, to minimize the effects of the interstellar reddening which are much more pronounced in the I band than in J and K_S.

There are both random and systematic errors in our estimates of $m_{\rm bol}$. The random errors come from two sources, namely from the observational uncertainties in the observed J and K_S band magnitudes, and from the corresponding uncertainties in the $(J-K_S)$ color. We have calculated the resulting random errors in the $m_{\rm bol}$ estimates through propagation of these errors. There are also two sources of systematic error in the $m_{\rm bol}$ estimates. The first one derives from uncertainties in the dust extinction correction. Our treatment of dust extinction is discussed in Section 2.3; Appendix A.3.4 discusses how the uncertainties in this correction introduce a small systematic error on the TRGB magnitude determination. The second source of systematic error is due to possible systematic errors in the spectral energy distributions of the models themselves. For the models by Groenewegen & collaborators we estimate this systematic error to be 2 to 5% of the interpolated percentage of flux, which corresponds to the residual of the fit performed on the model data points in the (percentage,$J-K_S$) diagram. However, for stars near the TRGB the blackbody model is usually the relevant one. For the blackbody fit the systematic errors are probably smaller (for similar values of J and K_S), although we have not made a rigorous estimate of this systematic error. That would require a larger set of data, e.g., UBRI-JHKL photometry, or spectra. Based on the comparison of our bolometric corrections with those of Montegriffo et al., and on the differences that we obtain when comparing results based on I, J and K_S with those based on J and K_S only, we have included in our final error budget a systematic error of ± 0.05 mag in our $m_{\rm bol}$ estimates due to uncertainties in the underlying spectral model.

In our analysis of the TRGB magnitude we have propagated the random and systematic errors on $m_{\rm bol}$ separately. However, for illustrative purposes we show in Fig. 1d the combined error due to both sources. Note that the average error for stars near the TRGB (see Table 1) is smaller than for the brighter TP–AGB stars. This is because the former generally use the blackbody models, while the latter use the models by Groenewegen & collaborators.

2.3. Dust Extinction

The contribution of the internal reddening for the Magellanic Clouds is on average only $E(B-V) = 0.06$ while the foreground reddening can be very high in the outskirts of the Clouds. We have not attempted to correct our sample for extinction on a star by star basis. Instead we correct all data for one overall extinction. We adopt $E(B-V) = 0.15 \pm 0.05$ as the average of known measurements (Westerlund 1997) for both Clouds. Adopting the extinction law by Glass (1999) for the DENIS pass bands $[A_V : A_I : A_J : A_{K_S} = 1 : 0.592 : 0.256 : 0.089]$ and $R_v = 3.1$ we obtain $A_I = 0.27$, $A_J = 0.11$ and $A_{K_S} = 0.04$. Our approach to correct for dust extinction is a simple approximation to what is in reality a very complicated issue (e.g., Zaritsky 1999). We discuss the effect of uncertainties in the dust extinction on our results in Sections 4.4 and 5. While this is an important issue in the I band, the bolometric magnitudes that we use to determine the distance modulus are impacted only at a very low level.

3. The Luminosity Function

The luminosity function (LF) of a stellar population is a powerful tool to probe evolutionary events and their time scales. Major characteristics of a stellar population are associated to bumps, discontinuities and slope variations in the differential star counts as a function of magnitude. However, for a proper interpretation of observed luminos-

ity functions several important issues should be taken into account. These include the completeness of the sample of data, the foreground contamination with respect to the analyzed population, the photometric accuracy and the size of the sampling bins. The total number of objects involved plays an important role to make the statistics significant.

In most previous studies of the luminosity functions of stellar populations in clusters or galaxies, in either the optical or the NIR, limited statistics have been the main problem. The DENIS (Cioni et al. 2000a) and 2MASS (Nikolaev & Weinberg 2000) samples provide the first truly large statistical sample in the NIR of the Magellanic Cloud system. This wavelength domain is the most suitable to study late evolutionary stages such as the RGB and the AGB. In the present paper we restrict the discussion of the luminosity function mostly to the TRGB; a more general discussion is given elsewhere (Cioni, Messineo & Habing 2000).

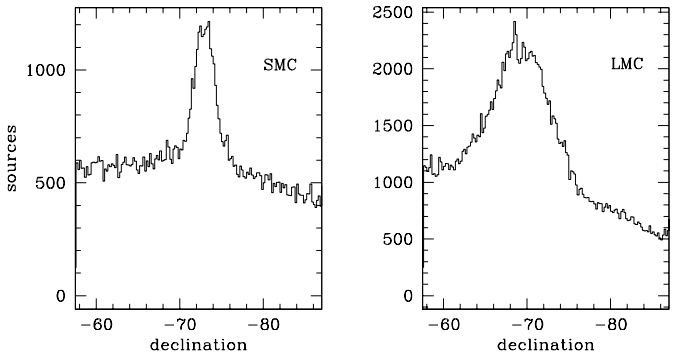

Fig. 2. Distribution of the sources in the sample versus declination using bins of 0.1 degrees, for the SMC (left) and the LMC (right).

3.1. The contribution of the Galaxy

For the removal of foreground contamination we considered two offset fields around each cloud. The range of right ascension (RA) is the same for both the cloud and the offset fields; it is the same of the DCMC catalogue (Section 2.1). For the LMC the north field has $-58° > \delta > -60°$ and the south field has $-80° > \delta > -86°$; for the SMC the north field has $-60° > \delta > -66°$ and the south field has $-80° > \delta > -86°$. The LMC region itself was limited to the declination range $-62° > \delta > -76°$, and the SMC region to $-69° > \delta > -77°$. Fig. 2 shows the distribution versus declination of the sources in the sample, using bins of 0.1 degrees. The foreground contribution clearly decreases toward more negative declinations, due to the difference in Galactic latitude. The difference in number between the foreground contribution around the LMC and around the SMC is consistent with the fact that the LMC is observed closer to the galactic plane than the SMC is. The structure of the LMC is clearly wider than the one of the SMC and this may contribute to create the strong declination trend around the LMC.

For each field and photometric band we constructed a histogram of the observed magnitudes (thin solid curves in the $N(m)$ panels of Fig. 3). For the two different offset fields at each right ascension range the data were combined into one histogram. This offset–field histogram (thin dashed curves) was then scaled to fit the corresponding LMC or SMC field histogram at bright magnitudes, for which almost all the stars belong to the foreground. Subtraction yields the foreground–subtracted magnitude distribution for each of the Clouds (heavy solid curves). For comparison we also extracted from the catalogue an extended sample consisting of those stars detected in the I and J bands (irrespective of whether or not they were detected in K_S). This sample (heavy dashed curves) is complete to fainter magnitudes than the main sample, and therefore illustrates the completeness limit of the main sample.

3.2. The shape

The resulting statistics of the subtracted LF are impressive, despite the restricted source selection. We proceed with a description of the major characteristics of the LF. The maximum corresponds to giants that lie on the upper part of the RGB. The decrease at fainter magnitudes is due to the selections applied to the data and to the decrease in sensitivity of the observations (Cioni et al. 2000a). Features like the horizontal branch or the red clump are too faint to be detected by DENIS. Towards brighter magnitudes we encounter a strong kink in the profile, which we associate with the position of the TRGB discontinuity. Brightward of the kink follows a bump of objects which we discuss below. At very bright magnitudes the LF has a weak tail which is composed of stars of luminosity type I and II (Frogel & Blanco 1983), but the LF at these bright magnitudes could be influenced by small residuals due to inaccurate foreground subtraction.

To explain the bump brightward of the TRGB discontinuity we cross–identified (Loup 2000) the DCMC sources with the sources in some of the Blanco fields in the LMC (Blanco 1980). In the $(K_S, J-K_S)$ diagram there are two regions populated only by oxygen rich AGB stars (O–rich) and by carbon rich AGB stars (C–rich), respectively. O–rich stars are concentrated around $K_S = 11.5$ and have a constant color $(J-K_S) = 1.2$, and C–rich stars are concentrated around $(J-K_S) = 1.7$ and around $K_S = 10.5$ (see Fig. 5b). These TP–AGB stars cause the bump visible in the LF. This bump should not be confused with the AGB bump caused by E–AGB stars (Gallart 1998). Fig. 4 shows an enlargement of Figs. 3c and 3k (continuous line). The dashed line refers to O–rich AGB stars and the dotted line to C–rich AGB stars selected in the $(K_S, J-K_S)$ diagram. In the case of the SMC we selected regions with slightly bluer color and fainter magnitude to

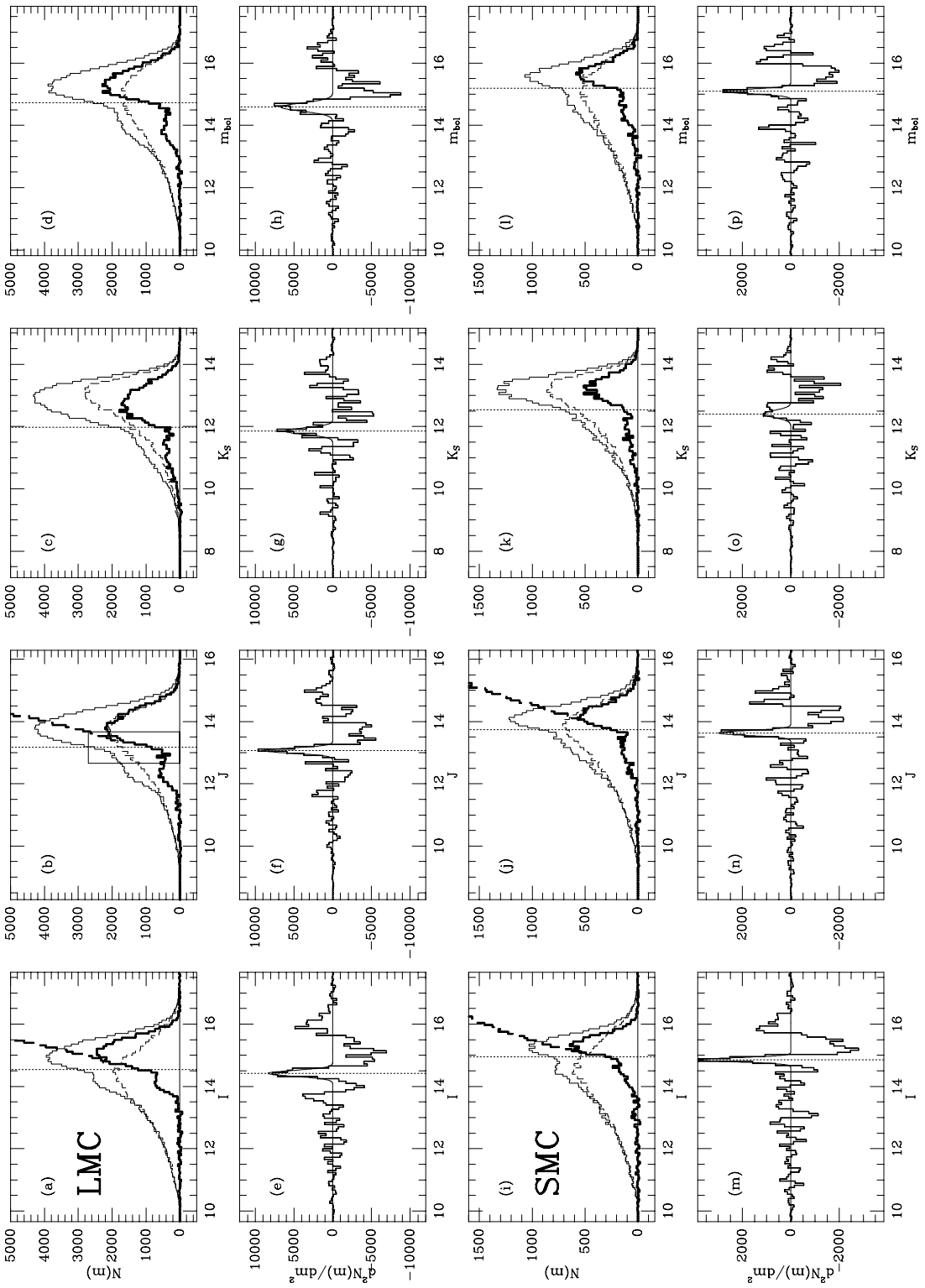

Fig. 3. Stellar magnitude distributions, $N(m)$, and second derivative after the application of a Savitzky-Golay filter, $\mathrm{d}^2N(m)/\mathrm{d}m^2$, for the LMC (a–h) and the SMC (i–p). Panels (a–d) and (i–l) show the distributions for the main field (thin solid curve), for the scaled offset field (thin dashed curve), and for the foreground–subtracted main field (heavy solid curve). For the I and J bands we also show the distribution for the foreground–subtracted main field for the larger sample of all stars detected in I and J (irrespective of K_S; heavy long–dashed curves). The final estimate of the TRGB discontinuity is indicated (vertical dotted line). The unit along the ordinate is the number of stars per 0.07 mag bin. Panels (e–h) and (m–p) show the second derivative for the foreground–subtracted main field (heavy solid curve), the best Gaussian fit to the peak (thin solid curve), and the position of the peak (vertical dotted line). The solid rectangle in (b) outlines the region shown in detail in Fig. A1.

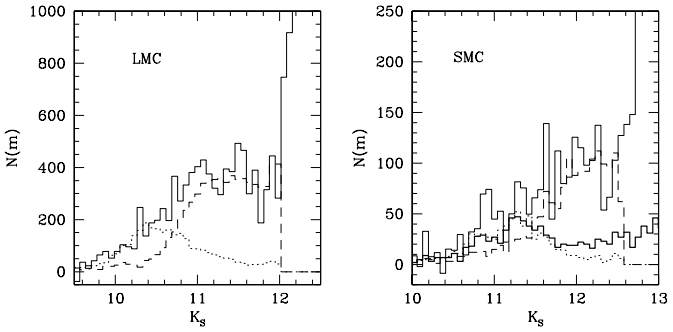

Fig. 4. Differential count of the number of sources detected versus magnitude in the area of the Magellanic Clouds after the subtraction of the foreground contribution (thin solid line). This enlarges part of Figs. 3c and 3m. The curves show the contributions of O–rich AGB stars (dashed), C–rich TP–AGB stars (dotted), and spectroscopically confirmed C–rich AGB stars (thick solid for the SMC only).

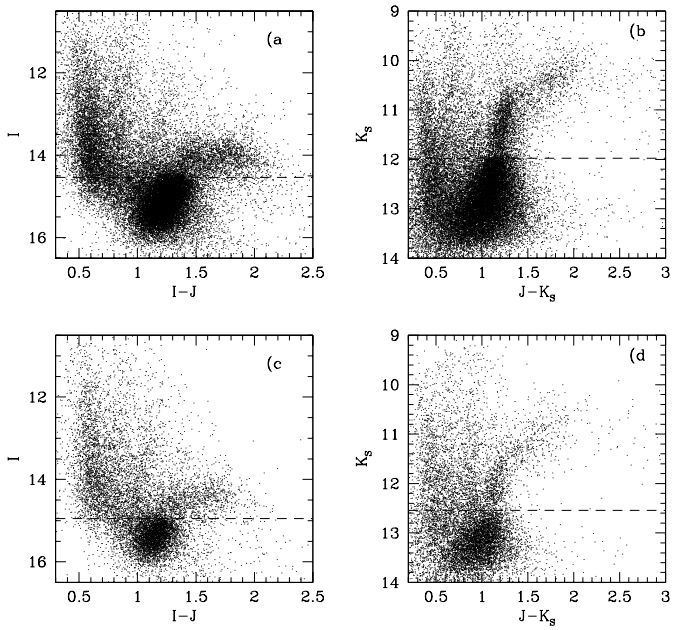

Fig. 5. Color–magnitude diagrams of $(I, I-J)$ on the left and $(K_S, J-K_S)$ on the right for sources detected toward the LMC with $-67° > \delta > -69°$ (panels a and b) and toward the SMC with $-72° < \delta < -74°$ (panels c and d). A dashed horizontal line in each panel indicates the TRGB magnitude derived in Section 4 (Table 1).

match the two groups of AGB stars in the $(K_S, J-K_S)$ diagram, cf. Fig. 5d. Fig. 4 also plots the LF (thick line) that results when we cross–identify our sample with the spectroscopically confirmed carbon stars by Rebeirot et al. (1983) in the SMC. We found 1451 sources out of 1707 and we attribute the missing cross–identifications to the selection criteria that we applied to the DCMC data to obtain the sample for the present paper. It is interesting to note that at higher luminosities the distribution of the confirmed C–rich stars matches the distribution of C–rich stars selected only on the basis of K_S and $(J-K_S)$. At the fainter luminosities C–rich AGB stars cannot be discriminated from O–rich AGB stars only on the basis of $(J-K_S)$ and K_S because they overlap with the RGB, principally constituted by O–rich stars.

4. The tip of the RGB

4.1. Theory

Theoretically stars climb the RGB with an expanding convective envelope and an hydrogen burning shell, while increasing the core–Helium content, the central temperature, the central density, and the luminosity. Low–mass stars ($0.8-1.0M_\odot < M < 2-2.3M_\odot$) develop an electron–degenerate core, which causes an explosive start (Helium–flash) of the core–Helium burning when the core mass reaches $0.45M_\odot$, almost independently from the initial mass and composition of the star (Chiosi et al. 1992); intermediate mass stars ($2-2.3M_\odot < M < 8-9M_\odot$) are not affected by degeneracy at this stage and initiate helium quietly, when a suitable temperature and density are reached. The RGB transition phase between the two behaviors occurs when the population is at least 0.6 Gyr old and lasts roughly for 0.2 Gyr, determining an abrupt event in the population life time (Sweigart et al. 1990). The Helium–flash is followed by a sudden decrease in the luminosity because of the expansion of the central region of the star and because of the extinction of the hydrogen–burning shell, the major nuclear energy supply. The star reaches its maximum luminosity and radius (in the RGB phase) at the TRGB, which also marks the end of the phase itself (Iben 1967). Low–mass stars with the same metallicity accumulate along the RGB up to a TRGB luminosity of about $2500L_\odot$ (Westerlund 1997); the resulting RGB is quite extended. Stars with masses just above the transition mass (which discriminates between low and intermediate masses) have a TRGB luminosity as low as $200L_\odot$ (Sweigart et al. 1989, 1990) and the RGB is almost non–existent. Both low and intermediate mass stars that finish burning their Helium in the core evolve on the AGB phase. They are in the so called E–AGB when Helium is burning in a thick shell and in the so called TP–AGB when both the Hydrogen and the Helium shells are active. The luminosity increases because of the increase in mass of the degenerate carbon core. The AGB evolution is characterized by a strong mass loss process that ends the phase when the outer envelope is completely lost. The maximum AGB luminosity defines the tip of the AGB (TAGB), with core mass $M_{\rm core} = 1.4M_\odot$ and magnitude $M_{bol} = -7.1$ mag (Paczynski 1970).

4.2. Detections

In the observed diagrams $(I, I-J)$ and $(K_S, J-K_S)$ the RGB is clearly visible (Fig. 5). The beginning of the RGB phase is below the detection limits and the spread

Table 1. Summary of TRGB magnitude determinations and errors. Column (1): type of magnitude, i.e., either the photometric band or $m_{\rm bol}$. Listed magnitudes for I, J and K_S are in the photometric system of the DENIS passbands (Fouqué et al. 1999). Column (2): Cloud name. Column (3): observed magnitude of the TRGB (not corrected for extinction), determined using the algorithm described in Appendix A. Column (4): magnitude of the TRGB corrected for extinction under the assumption that $E(B-V)=0.15$. Column (5): formal error in $m_{\rm TRGB}$ derived from Monte-Carlo simulations as described in Appendix A. Column (6): the amount by which the extinction-corrected $m_{\rm TRGB}$ would change if the assumed $E(B-V)$ were increased by +0.05 (a change of −0.05 yields the opposite change in $m_{\rm TRGB}$).

Type	Cloud	$m_{\rm TRGB}$ (observed)	$m_{\rm TRGB}$ (dereddened)	$\Delta m_{\rm TRGB}$ (formal)	$\delta_{\rm dust}$
(1)	(2)	(3)	(4)	(5)	(6)
I	LMC	14.54	14.27	0.03	−0.09
I	SMC	14.95	14.68	0.03	−0.09
J	LMC	13.17	13.06	0.02	−0.04
J	SMC	13.73	13.62	0.03	−0.04
K_S	LMC	11.98	11.94	0.04	−0.02
K_S	SMC	12.54	12.50	0.07	−0.02
$m_{\rm bol}$	LMC	− − −	14.73	0.04	−0.03
$m_{\rm bol}$	SMC	− − −	15.19	0.03	−0.03

at the fainter magnitudes is due to the photometric errors. The TRGB is clearly defined at the brightest point of this branch as an outstanding roughly horizontal feature. Dashed horizontal lines in the figure indicate the values of the TRGB discontinuity that we derive below for these data. The plume of objects brighter than the TRGB is composed of AGB stars experiencing the TP phase. From these diagrams the foreground contribution has not been subtracted but the contamination of these to the RGB/AGB is negligible (Cioni et al. 1998, 2000a) if only the very central region of each cloud is selected; Fig. 5 contains sources with $-67^\circ > \delta > -69^\circ$ toward the LMC and $-72^\circ > \delta > -74^\circ$ toward the SMC. Stars populating the RGB up to the TRGB are low–mass stars older than 0.6 Gyr. TP–AGB stars on the other hand, which lie above the TRGB, can be either low–mass stars or intermediate mass–stars. For $M_{bol} < -6$ mag they all originate from main–sequence stars with $M < 3M_\odot$ (Westerlund 1997), which corresponds to a minimum age of 0.2 Gyr. TP–AGB stars that are low–mass stars should be older than 1 Gyr (Vassiliadis and Wood 1993). Note that the thickness of the RGB (~ 0.3 mag) is larger than the photometric errors involved (~ 0.1 mag) and this indicates a spread in either metallicity or extinction within each cloud.

4.3. Method

The algorithm that we have used for the determination of the position of the magnitude $m_{\rm TRGB}$ of the TRGB is described in great detail in Appendix A. The TRGB discontinuity causes a peak in both the first derivative $N'(m) \equiv {\rm d}N(m)/{\rm d}m$ and the second derivative $N''(m) \equiv {\rm d}^2N(m)/{\rm d}m^2$ of the observed stellar magnitude distribution $N(m)$. Previous authors have generally used $N'(m)$ to estimate $m_{\rm TRGB}$ (e.g., Madore & Freedman 1995). Based on extensive tests and simulations we found that for our dataset $N''(m)$ provides a better handle on $m_{\rm TRGB}$ (cf. Appendix A.1). We therefore adopted the following approach. First, we use a Savitzky-Golay filter (e.g., Press et al. 1992) to estimate $N''(m)$. We then search for a peak in $N''(m)$, and fit a Gaussian to it to obtain the quantities m_{2g} and σ_{2g} that are the mean and dispersion of the best-fitting Gaussian, respectively. The magnitude $m_{\rm TRGB}$ is then estimated as $m_{2g}+\Delta m_{2g}(\sigma_{2g})$, where $\Delta m_{2g}(\sigma_{2g})$ is a small correction (Fig. A2b) derived from a phenomenological model described in Section A.1. The formal errors on the $m_{\rm TRGB}$ determinations are inferred from extensive Monte-Carlo simulations, as described in Section A.2. The possible influence of systematic errors is discussed in Section A.3. There is no evidence for any possible systematic errors due to possible incompleteness in the sample, or inaccuracies in the foreground subtraction. Systematic errors due to uncertainties in the phenomenological model on which the corrections $\Delta m_{2g}(\sigma_{2g})$ are based can be up to ± 0.02 magnitudes. Extinction variations within the Clouds do not cause systematic errors in either the estimate of $m_{\rm TRGB}$ or its formal error. However, any error in the assumed *average* extinction for the sample does obviously translate directly into an error in $m_{\rm TRGB}$.

Fig. 3 summarizes the results of the analysis. The second and fourth row of the panels show the estimates of $N''(m)$. The Gaussian fit to the peak is overplotted, and its center m_{2g} is indicated by a vertical dotted line. The corresponding estimate $m_{\rm TRGB}$ is indicated by a vertical dotted line in the panel for $N(m)$. Table 1 lists the results. It includes both the observed value for $m_{\rm TRGB}$, as well as the value obtained after correction for extinction with $E(B-V)=0.15$. Formal errors are listed as well, and are typically 0.03–0.04 magnitudes. The last column of the Table lists the amount by which the extinction-corrected $m_{\rm TRGB}$ would change if the assumed $E(B-V)$ were increased by +0.05 (a shift of −0.05 in the assumed $E(B-V)$ would produce the opposite shift in $m_{\rm TRGB}$).

When applying comparable methods to resolvable galaxies in the Local Group (e.g., Soria et al 1996; Sakai et al. 1996) one of the major sources of contamination on the TRGB determination is the presence of a relative strong AGB population. The Magellanic Clouds also have a strong AGB population, but in our case this does not confuse the determination of $m_{\rm TRGB}$. This is due to

the large statistics available, and above all to the fact that TP–AGB stars are definitely more luminous than the TRGB. E–AGB stars overlap with the RGB stars but there is no reason to assume, according to models, that they accumulate at the TRGB. Probably they distribute rather constantly and due to the very short evolutionary time scale we do not expect them to exceed more than 10% of the RGB population.

4.4. Discussion

The absolute magnitude of the TRGB generally depends on the metallicity and the age of the stellar population and therefore need not to be the same for the LMC and the SMC. Nonetheless, if we assume that such differences in TRGB absolute magnitude are small or negligible, and if we assume that the extinction towards the LMC and the SMC have been correctly estimated, then one may subtract for each photometric band the inferred $m_{\rm TRGB}$(LMC) from the inferred $m_{\rm TRGB}$(SMC) to obtain an estimate of the difference $\Delta \equiv (m-M)_{\rm SMC} - (m-M)_{\rm LMC}$ between the distance moduli of the SMC and the LMC. This yields the following results: 0.41 ± 0.04 (I band), 0.56 ± 0.04 (J band), 0.56 ± 0.08 (K_S band) and 0.46 ± 0.05 ($m_{\rm bol}$). The dispersion among these four numbers is 0.06, which is consistent with the formal errors. This indicates that the formal errors are likely to be accurate (and at least are not underestimates), and also that any difference in the TRGB absolute magnitudes between the Clouds probably does not significantly exceed the formal errors. Averaging the four determinations yields the $\Delta = 0.50 \pm 0.03$, where the error is the formal error in the mean. This agrees well with determinations found in the literature, which generally fall in the range $\Delta = 0.4$—0.5 (Westerlund 1997).

Upon taking a closer look at the values of Δ for the different bands one sees that the values in J and K_S exceed those in I by 0.15 mag. It is quite possible that this is due to differences in the metallicity and age of the LMC and the SMC, which affect the TRGB absolute magnitude $M_{\rm TRGB}$ differently in different bands. In the I band $M_{\rm TRGB}$ is reasonably insensitive to metallicity and age. Lee et al. (1993) showed that $M_{\rm TRGB}(I)$ changes by less than 0.1 mag for $-2.2 < [Fe/H] < -0.7$ dex and for ages between 2 and 17 Gyr. For the K band, Ferraro et al. (1999) derived an empirical relation between $M_{\rm TRGB}(K)$ and the metallicity in galactic globular clusters. For metallicities in the range of the Magellanic Clouds the variation of $M_{\rm TRGB}(K)$ is about 0.2 mag; however, this relation might not be valid for intermediate age populations. From the theoretical isochrones by Girardi et al. (2000) the spread of $M_{\rm TRGB}(K)$ is about 0.3 mag for ages greater than 2 Gyr and constant metallicity. This spread is somewhat less for the J band but it remains higher than the one derived for the I band. The fact that $M_{\rm TRGB}$ is modestly sensitive to variations in metallicity and age for the J and K bands implies that the values of Δ derived in these bands may not be unbiased estimates of the true difference in distance modulus between the SMC and the LMC. The I band value should be better in this respect, but on the other hand, that value is more sensitive to possible differences in the dust extinction between the Clouds. So the best estimate of Δ is probably obtained using $m_{\rm bol}$, as discussed further in Section 5.

For the LMC there are several observed TRGB magnitude determinations in the literature that can be compared to our results. Reid et al. (1987) obtained $m_{\rm TRGB}(I) = 14.53 \pm 0.05$, after extinction-correction with an assumed $A_I = 0.07$. Romaniello et al. (1999) obtained $m_{\rm TRGB}(I) = 14.50 \pm 0.25$ for the field around SN1987A. They corrected each star individually for extinction, but found a mode of $E(B-V) = 0.20$ for their sample (corresponding to $A_I = 0.30$). Sakai et al. (1999) obtained $m_{\rm TRGB}(I) = 14.54 \pm 0.04$. They also corrected each star individually for extinction, but restricted their sample to low-extinction regions with $A_V < 0.2$ (corresponding to $A_I < 0.10$). The observed value of $m_{\rm TRGB}(I)$ for our sample, 14.54 ± 0.03, is nicely consistent with all these determinations. However, when we apply an extinction correction of $A_I = 0.27$, as appropriate for an assumed $E(B-V) = 0.15$ (Section 2.3), our corrected value falls significantly below the previous determinations. This may mean that our assumed extinction is an overestimate. Support from this comes from a recent study by Zaritsky (1999). He demonstrates that the average extinction towards cool stars is much lower than for the hotter stars which have typically been used to estimate the extinction towards the LMC (the latter generally reside in star-forming regions which are more dusty, among other things). The analysis of Zaritsky (cf. his Fig. 12) suggests that the mode of the distribution of A_V for stars with temperatures appropriate for the RGB is as low as $A_V \approx 0.1$ (corresponding to $A_I \approx 0.05$), but with a long tail towards higher extinctions. Either way, it is clear that any proper interpretation of the TRGB magnitude in the I band requires an accurate understanding of the effects of dust extinction. We have not (yet) performed such an extinction analysis for our sample, and therefore refrain from drawing conclusions from our I band results. However, our results are not inconsistent with observations by previous authors, provided that the extinction is actually as low as suggested by Zaritsky.

The best way to circumvent any dependence of the results on uncertainties in the dust extinction is to go far into the near IR. There is one very recent determination of $m_{\rm TRGB}$ in the K_S band that can be compared to our results. Nikolaev & Weinberg (2000) used data from the 2MASS survey to derive $m_{\rm TRGB}(K_S) = 12.3 \pm 0.1$, without correcting for extinction. Somewhat surprisingly, this exceeds our determination $m_{\rm TRGB}(K_S) = 11.98 \pm 0.04$ by as much as 0.32 magnitudes. This cannot be attributed to differences in the definitions of the photometric sys-

tems used by the DENIS and 2MASS surveys. Neither system is identical to the standard CTIO K magnitude system, but both are quite close. Nikolaev & Weinberg quote that their K_S magnitude system agrees with the standard K to within 0.05 mag. For the DENIS system the final transformation equations will not be available until the survey is completed, but the analysis of Fouqué et al. (1999) yields an absolute flux zero-point (in Jy) for the DENIS K_S system that differs from the CTIO K-band by 0.08 mag. To further test the agreement of our magnitude system with that of 2MASS we compared our LMC K_S histogram to that presented by Nikolaev & Weinberg. Visual comparison shows excellent agreement to within 0.1 magnitudes or better. The comparison does show that our data become incomplete at brighter magnitudes than the 2MASS data does. However, tests discussed in Appendix A.3.2 show that our determinations of $m_{\rm TRGB}$ are not influenced by possible incompleteness near the TRGB in any significant way. So we are forced to conclude that the 0.32 mag difference in $m_{\rm TRGB}$ must be due to differences in how $m_{\rm TRGB}$ is defined and determined, and not to differences in the data themselves. While we search for a peak in $N''(m)$ and then add a correction term that is based on a model, Nikolaev & Weinberg just determine the peak in the first derivative $N'(m)$. As discussed in Section A.1 (see Fig. A2) this generally yields on overestimate of the actual TRGB magnitude. Since Nikolaev & Weinberg do not describe their analysis technique in detail, it is difficult to estimate the size of this bias in their result. However, Monte-Carlo simulations that we discuss in Section A.4 indicate that it could be $\sim 0.15 \pm 0.06$, which would explain at least part of the observed discrepancy. Note that the same effect may also affect some of the I band comparisons listed above, although for those the influence of extinction probably plays the more significant role.

5. Distance to the Magellanic Clouds

To estimate the distance modulus of the Magellanic Clouds we can use the observed magnitude of the TRGB in either I, J, K_S or $m_{\rm bol}$. As discussed in Section 4.4, I has the disadvantage of being sensitive to uncertain extinction corrections, while J and K_S have the disadvantage of being sensitive to the assumed metallicity and age. The most accurate information on the distance is therefore provided by m_{bol}, which is not particularly sensitive to either dust extinction (cf. Table 1) or metallicity and age. To quantify the latter we use the stellar evolutionary model calculations of Salaris & Cassisi (1998). They quantified the dependence of $M_{\rm TRGB}$(bol) on the total metallicity ($[M/H]$) of a population, and found that

$$M_{\rm TRGB}({\rm bol}) = -3.949 - 0.178[M/H] + 0.008[M/H]^2, \quad (1)$$

valid for $-2.35 < [M/H] < -0.28$ and for ages larger than a few Gyr.

We determined $[M/H]$ by qualitatively fitting isochrones (Girardi et al. 2000) to the color–magnitude diagram $(K_S, J-K_S)$. We obtain $Z = 0.004 \pm 0.002$ for the LMC, in agreement with the value derived by Nikolaev & Weinberg, and $Z = 0.003 \pm 0.001$ for the SMC. For $Z_\odot = 0.02$ this corresponds to $[M/H] = -0.70$ and $[M/H] = -0.82$ for the LMC and the SMC, respectively. This in turn yields $M_{\rm TRGB}({\rm bol}) = -3.82$ for the LMC and $M_{\rm TRGB}({\rm bol}) = -3.80$ for the SMC. When combined with the results in Table 1 we obtain for the LMC that $(m-M) = 18.55 \pm 0.04$ (formal) ± 0.08 (systematic), and for the SMC that $(m-M) = 18.99 \pm 0.03$ (formal) ± 0.08 (systematic). The corresponding distances are 51 and 63 kpc to the LMC and the SMC respectively.

The systematic errors that we quote in our results are the sum in quadrature of the following possible (identified) sources of error: (i) ± 0.02 mag due to uncertainties in the phenomenological model on which the corrections $\Delta m_{2g}(\sigma_{2g})$ are based (cf. Section A.3.1); (ii) ± 0.03 mag to account for the fact that our assumed average dust extinction of $E(B-V) = 0.15$ could plausibly be in error by 0.05 (cf. Table 1); (iii) ± 0.04 mag, reflecting the uncertainties in $M_{\rm TRGB}$(bol) due to uncertainties in $[M/H]$; (iv) ± 0.04 mag, reflecting the uncertainty in $M_{\rm TRGB}$(bol) at fixed $[M/H]$ suggested by comparison of the predictions of different stellar evolution models (Salaris & Cassisi 1998; their Fig. 1); (v) ± 0.05 mag, being an estimate of the possible systematic error in our calculation of bolometric magnitudes due to uncertainties in the underlying spectral model (see Section 2.2)..

There have been many previous determinations of the distance modulus of the LMC, and these have varied widely, from about 18.0 to 18.7. Based on a collection of many determinations, the HST Key Project Team adopted $(m-M) = 18.50 \pm 0.13$ (Mould et al. 2000). Our determination is in excellent agreement with this value, and actually has a smaller error. The TRGB method itself has been used previously by several other authors to study the distance modulus of the LMC, and our results are consistent with all of these. Reid, Mould & Thompson (1987) were the first to apply this technique to the LMC (by studying the Shapley Constellation III using photographic plates), and obtained $(m-M) = 18.42 \pm 0.15$. Romaniello et al. (1999) obtained $(m-M) = 18.69 \pm 0.25$ from a field around SN1987A in the LMC using HST/WFPC2 data. Sakai et al. (1999) obtained 18.59 ± 0.09 from an area of 4×2.7 square degrees (north of the LMC bar) studied as part of the Magellanic Cloud Photometric Survey (Zaritsky, Harris & Thompson 1997) using the Las Campanas 1m telescope. Nikolaev & Weinberg (2000) obtained $(m-M) = 18.50 \pm 0.12$ from the subset of 2MASS data that covers the LMC. For the SMC we are not aware of (recent) TRGB distance modulus measurements, but our result is consistent with the value $(m-M) = 18.90 \pm 0.10$ quoted by Westerlund (1997) from a combination of mea-

surements available in the literature from a variety of techniques.

6. Conclusions

We have determined the position of the TRGB for both Magellanic Clouds using the large statistical sample offered by the DCMC (Cioni et al. 2000a). We have presented a new algorithm for the determination of the TRGB magnitude, which we describe in detail in the Appendix and test extensively using Monte-Carlo simulations. We note that any method that searches for a peak in the first derivative (used by most authors) or the second derivative (used by us) of the observed luminosity function does not yield an unbiased estimate for the actual magnitude of the TRGB discontinuity. We stress the importance of correcting for this bias, which is not generally done. Our analysis shows that when large enough statistics are available, contamination by AGB stars does not provide a significant limitation to the accuracy of the TRGB magnitude determination.

In our analysis we have adopted global values for the extinction of the Magellanic Clouds and we have derived the metallicity from an isochrone fit to the giant population to obtain a representative value for each cloud as a whole. In reality, extinction and metallicity are likely to vary within each cloud. Clearly, the production of a detailed extinction map together with precise measurements of the metallicity is a requirement for a detailed analysis of variations in structure between different locations within the Clouds, either on the plane of the sky or along the line of sight. However, such variations do not influence our distance determinations, which should be accurate in a globally averaged sense. Uncertainties in the average dust extinction or metallicity for each cloud are included in the systematic error budget of our final estimates.

We combine our apparent bolometric TRGB magnitude determinations with theoretical predictions to derive the distance modulus of the Clouds. We obtain $(m-M) = 18.55 \pm 0.04$ (formal) ± 0.08 (systematic) for the Large Magellanic Cloud (LMC), and $(m-M) = 18.99 \pm 0.03$ (formal) ± 0.08 (systematic) for the Small Magellanic Cloud (SMC). These results are consistent with many previous studies, including a recent compilation by Mould et al. (2000). However, only very few previous studies have yielded determinations of similar accuracy as those presented here. This re-confirms the TRGB method to be a high quality method for distance determination of resolved stellar populations, and stresses the power of large statistical samples in the NIR such as those provided by the DENIS survey.

Appendix A: Determination of the TRGB magnitude: methodology and error analysis

A.1. The nature of the TRGB discontinuity

We wish to determine the magnitude $m_{\rm TRGB}$ of the TRGB discontinuity from an observed magnitude distribution $f_{\rm obs}(m)$. In general, the observed distribution will be the convolution of the intrinsic magnitude distribution of the stars, $f_{\rm int}(m)$, with some broadening function $E(m)$:

$$f_{\rm obs}(m) = \int_{-\infty}^{\infty} f_{\rm int}(m') E(m-m')\,{\rm d}m'. \quad \text{(A1)}$$

The function $E(m)$ characterizes the probability that a star with magnitude m_0 is observed to have magnitude $m_{\rm obs} = m_0 + m$. The shape of $E(m)$ is generally determined by the properties of the observational errors, but other effects (such as differences in extinction or distance among the stars in the sample) can contribute as well.

To gain an understanding of the issues involved in the determination of $m_{\rm TRGB}$ we start by considering a simple model. We assume that $E(m)$ is a Gaussian of dispersion σ:

$$E(m) = \frac{1}{\sqrt{2\pi}\,\sigma}\, e^{-\frac{(m/\sigma)^2}{2}}. \quad \text{(A2)}$$

We approximate $f_{\rm int}(m)$ by expanding it into a first-order Taylor expansion near the position of the discontinuity, which yields

$$f_{\rm int}(m) = \begin{cases} f_0 + a_1(m - m_{\rm TRGB}), & \text{if } m < m_{\rm TRGB}\ ; \\ f_0 + \Delta f + a_2(m - m_{\rm TRGB}), & \text{if } m > m_{\rm TRGB}\ . \end{cases} \quad \text{(A3)}$$

The parameters a_1 and a_2 measure the slope of $f_{\rm int}$ for magnitudes that are brighter and fainter than $m_{\rm TRGB}$, respectively. At brighter magnitudes the sample is dominated by AGB stars, while at fainter magnitudes both AGB and RGB stars contribute. The parameter Δf measures the size of the discontinuity; the ratio $\Delta f / f_0$ is an estimate of the ratio of the number of RGB to AGB stars at the magnitude of the RGB tip.

We fitted the model defined by Eqs. (A1)–(A3) to the observed (foreground-subtracted) J band magnitude histogram for the LMC, which is shown as a connected heavy dashed curve in Fig. A1a. The heavy solid curve shows the model distribution $f_{\rm obs}$ that provides the best fit. The fit is acceptable. The parameters for this model are: $f_0 = 0.091$, $\Delta f = 0.250$ (both in units in which the normalization of f is arbitrary), $a_1 = -0.108$, $a_2 = 0.928$, $m_{\rm TRGB} = 13.16$ and $\sigma = 0.126$. The long-dashed curve shows the underlying distribution $f_{\rm int}(m)$ for this model. For these J band data we know that the magnitude errors are dominated by photometric zero–point variations between the scan-strips that constitute the LMC sample (Cioni et al. 2000a). These variations have a dispersion of 0.13 (which significantly exceeds the formal photometric errors near the TRGB magnitude, cf. Fig. 1). In view of

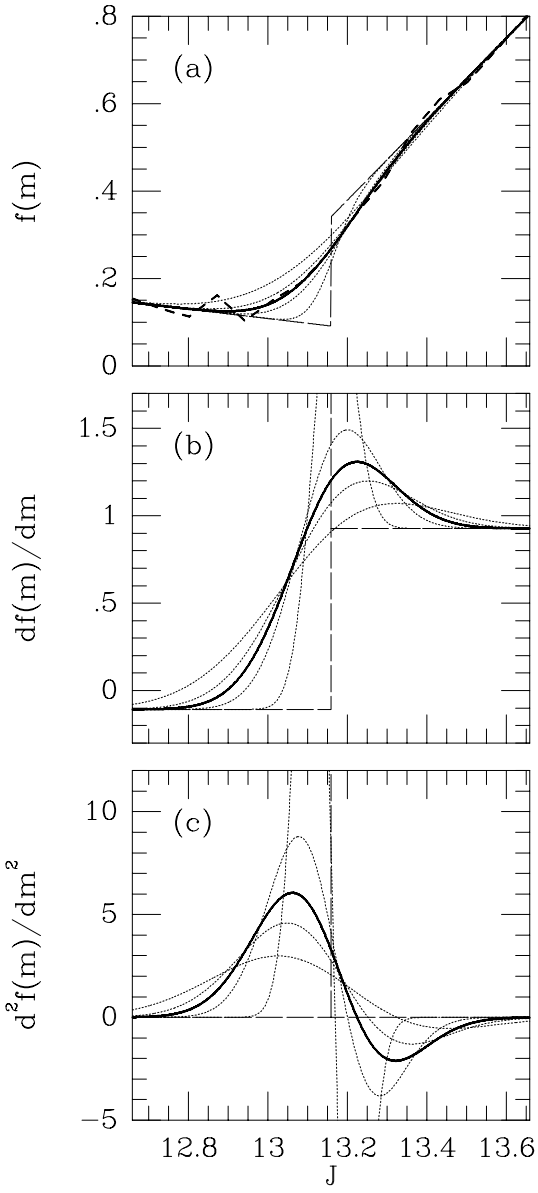

Fig. A1. (a) The connected heavy dashed curve shows the foreground-subtracted LMC J band magnitude distribution (thus providing an expanded view of the region indicated by a rectangle in the LMC J band panel in Fig. 3) for the expanded sample of stars detected in the I and J bands (irrespective of whether or not they were detected in K_S). This sample is complete over the displayed magnitude range. The heavy solid curve shows the distribution predicted by the model described in the text. This model has the intrinsic distribution $f_{\rm int}(m)$ shown as a thin long-dashed curve, and has an observational convolution kernel $E(m)$ that is a Gaussian with a dispersion $\sigma = 0.126$. For comparison, thin dotted curves show the predictions obtained when the same intrinsic distribution $f_{\rm int}(m)$ is convolved with Gaussians of size σ of 0.05, 0.10, 0.15 and 0.20, respectively. **(b)** The first derivative of the functions shown in panel (a). **(c)** The second derivative of the functions shown in panel (a). Note that the discontinuity at the TRGB induces a peak in both the first and the second derivative.

this, the value $\sigma = 0.126$ inferred from the model fit is very reasonable.

Model fitting can be used as a general tool to estimate $m_{\rm TRGB}$ from an observed magnitude distribution. However, this technique is error-prone, since one is essentially solving a deconvolution problem in which neither the exact shape of the intrinsic magnitude distribution $f_{\rm int}(m)$ nor that of the kernel $E(m)$ is well known a priori. A more robust approach is to locate a feature in the observed distribution $f_{\rm obs}(m)$ that is a direct consequence of the discontinuity at $m_{\rm TRGB}$. Since a discontinuity corresponds (by definition) to an infinitely steep gradient, one obvious approach is to search for a maximum in the first derivative $f'_{\rm obs} \equiv {\rm d}f_{\rm obs}/{\rm d}m$. This approach has been used in several previous studies of TRGB magnitude determinations (e.g., Lee, Freedman & Madore 1993). For a model with $a_1 = a_2 \equiv a$ one can show that one expects simply $f'_{\rm obs}(m) = a + \Delta f E(m - m_{\rm TRGB})$, i.e., the first derivative is a Gaussian centered at $m_{\rm TRGB}$ plus a constant. However, the above analysis shows that $a_1 \neq a_2$. So while the derivative $f'_{\rm obs}$ generally does have a maximum near $m_{\rm TRGB}$, the structure of the first derivative is generally more complicated than a Gaussian. The heavy curve in Fig. A1b shows $f'_{\rm obs}(m)$ for the model with the parameters determined from the J band data.

The magnitude distribution of stars on the AGB is very different from that on the RGB. While the former is approximately constant and in fact even slightly increasing to brighter magnitudes ($a_1 < 0$), the latter increases very sharply to fainter magnitudes ($a_2 > 0$). Hence, not only $f_{\rm int}$, but also its derivative is discontinuous at $m_{\rm TRGB}$. This corresponds to an infinitely steep gradient in the first derivative (see the long dashed curves in Fig. A1), which can be identified by searching for a maximum in $f''_{\rm obs} \equiv {\rm d}^2 f_{\rm obs}/{\rm d}m^2$. For a model with $\Delta f = 0$ one can show that one expects simply that $f''_{\rm obs}(m) = (a_2 - a_1) E(m - m_{\rm TRGB})$, i.e., the second derivative is a Gaussian centered at $m_{\rm TRGB}$. While the above discussion shows that the best fit to the data is obtained for $\Delta f \neq 0$, the value of Δf is close enough to zero to ensure that $f''_{\rm obs}(m)$ is always modestly well approximated by a Gaussian (especially near its peak). Fig. A1c shows $f''_{\rm obs}$ for the model with the parameters determined from the J band data.

While the discontinuity in $f_{\rm int}$ causes both a maximum in $f'_{\rm obs}$ at a position m_1 and a maximum in $f''_{\rm obs}$ at a position m_2, it is important to realize that neither provides a unbiased estimate of $m_{\rm TRGB}$. Fig. A2a shows for the model derived from the J band data the differences $\Delta m_1 \equiv m_1 - m_{\rm TRGB}$ and $\Delta m_2 \equiv m_2 - m_{\rm TRGB}$ as function of σ. In absolute value, the differences increase monotonically with σ. The value of m_1 always provides an overestimate of $m_{\rm TRGB}$ while m_2 always provides an underestimate. It is important to realize that in practice, because of finite statistics, one must always apply a certain amount of smoothing to real data to obtain an adequate

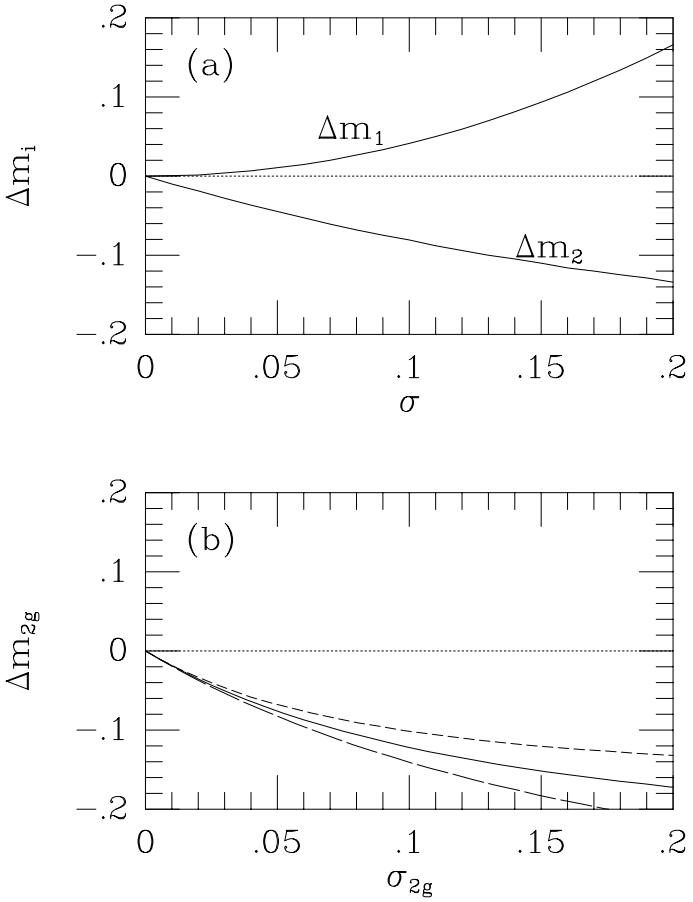

Fig. A2. (a) The differences $\Delta m_1 \equiv m_1 - m_{\rm TRGB}$ and $\Delta m_2 \equiv m_2 - m_{\rm TRGB}$ as function of σ, for models with the intrinsic magnitude distribution shown in Fig. A1. The quantities m_1 and m_2 are, respectively, the magnitudes at which the first and second derivatives of the observed magnitude distribution have their peak, while $m_{\rm TRGB}$ is the magnitude of the actual TRGB discontinuity. The quantity σ is the dispersion of the observational convolution kernel $E(m)$. **(b)** The difference $\Delta m_{2g} \equiv m_{2g} - m_{\rm TRGB}$ as function of σ_{2g}, where m_{2g} and σ_{2g} are the mean and dispersion of the Gaussian that best fits the peak in $f''_{\rm obs}(m)$. The solid curve refers to the same models as in (a), and provides the correction term that we have applied to the observed m_{2g} to obtain estimates of $m_{\rm TRGB}$. The other curves are for models with $\Delta f = 0.18$ (dashed) and $\Delta f = 0.38$ (long-dashed) in Eq. A3; as discussed in Section A.3.1, the differences between these curves and the solid curve provide an estimate of possible systematic errors in our results due to uncertainties in the adopted model for $f_{\rm int}(m)$.

estimate of either $f'_{\rm obs}$ or $f''_{\rm obs}$. This smoothing usually takes the form of binning (e.g., Lee, Freedman & Madore 1993)) or kernel smoothing (e.g., Sakai, Madore & Freedman 1996). When assessing the size of the bias terms in Fig. A2a for any particular application, the value of σ along the abscissa should therefore not be taken merely as the average photometric error for the data, but should include the effect of the additional smoothing that was applied to obtain the estimate of either m_1 or m_2. While photometric errors of a few hundredths of a magnitude are often routinely achieved, the additional smoothing or binning applied during data processing is often as large as 0.1 to 0.2 magnitudes. According to Fig. A2a, this can induce systematic biases in the estimate of $m_{\rm TRGB}$ that are of the same order. So while this is not typically done (e.g., Sakai, Zaritsky & Kennicutt 1999; Nikolaev & Weinberg 2000), we do believe that such systematic biases should be calculated and corrected for.

Previous authors have generally searched for the magnitude of the TRGB by determining the position of the peak in $f'_{\rm obs}$. As far as we know, no one has yet used $f''_{\rm obs}$. This is presumably for the obvious reason that it is more difficult to determine the second derivative from noisy data than the first derivative. However, the situation for the DCMC catalogue differs considerably from that for most other studies. First, we have a very large number of stars, so that it is actually not a problem to accurately determine $f''_{\rm obs}$. Second, the random errors in the sample are relatively large. This is not because of photometric errors (which are small, cf. Fig. 1) but because of photometric zero–point variations between the scan-strips that constitute the sample. The effect of the size of the errors on the properties of $f'_{\rm obs}$ and $f''_{\rm obs}$ are illustrated by the dotted curves in Fig. A1, which show predictions for the same model as before, but for values of σ of 0.05, 0.10, 0.15 and 0.20, respectively. We have found that the values of σ appropriate for our analysis are such that the peak in $f'_{\rm obs}(m)$ is generally not the most easily recognizable feature in the data. After extensive testing we concluded that for our data $f''_{\rm obs}(m)$ provides a better handle on $m_{\rm TRGB}$ than does $f'_{\rm obs}(m)$.

In practice, we estimate the properties of the peak in $f''_{\rm obs}(m)$ by performing a Gaussian fit. This yields m_{2g}, the center of the best-fitting Gaussian, and σ_{2g}, the dispersion of the best-fitting Gaussian (in general, the value of σ_{2g} is roughly of the same order as σ, and Δm_{2g} is roughly of the same order as Δm_2). For given $f_{\rm int}$, both m_{2g} and σ_{2g} are unique monotonic functions of σ. So one can view $\Delta m_{2g} \equiv m_{2g} - m_{\rm TRGB}$ to be a function of σ_{2g}. The solid curve in Fig. A2b shows this function for the $f_{\rm int}$ parameterization derived from the J band data.

A.2. Implementation and formal errors

To implement our strategy we bin the observed stellar magnitudes for the region of the sky of interest into a histogram, using a fixed bin size b. As described in Section 3.1, we do the same for observations of an offset field, and subtract an appropriately scaled version of the offset field histogram from the main field histogram to obtain a foreground-subtracted histogram $N(m)$. We then apply a Savitzky-Golay filter (e.g., Press et al. 1992) to estimate

the second derivative $\mathrm{d}^2N(m)/\mathrm{d}m^2$ at the position of each bin. This yields for bin number i

$$[\mathrm{d}^2N/\mathrm{d}m^2]_i = \sum_{j=-J}^{J} c_j\,[N(m)]_{i+j}, \tag{A4}$$

where the c_j are Savitzky-Golay coefficients for the chosen value of J and the desired derivative order $L = 2$. The filter fits a polynomial of order M to the data points $[N(m)]_j$ with $j = i-J, \ldots, i+J$, and then evaluates the L^{th} derivative of the polynomial at bin i to estimate $[\mathrm{d}^2N/\mathrm{d}m^2]_i$. Once a histogram approximation to $[\mathrm{d}^2N/\mathrm{d}m^2]$ has been calculated, we search for a peak and fit a Gaussian in the region around the peak to obtain m_{2g} and σ_{2g} (the mean and dispersion of the best-fitting Gaussian). From these values we estimate the magnitude m_{TRGB} as

$$m_{\mathrm{TRGB}} = m_{2g} - \Delta m_{2g}(\sigma_{2g}), \tag{A5}$$

where the correction term $\Delta m_{2g}(\sigma_{2g})$ is taken from Fig. A2c. To summarize, m_{TRGB} is estimated as the position where the second derivative of the observed histogram has its maximum, plus a small correction that is based on a model for the underlying magnitude distribution f_{int}.

We performed extensive Monte-Carlo simulations to assess the accuracy of the m_{TRGB} estimates produced by this algorithm. In these simulations Cloud stars are drawn from the magnitude distribution f_{int} given by Eq. (A3), using as before the parameters determined from the J band data. Foreground stars are drawn from a smooth magnitude distribution that matches that inferred from our data, both for the main field and a hypothetical offset field. To each stellar magnitude an error is added that is drawn from a Gaussian with dispersion σ. The numbers of stars in the simulations were chosen to match those in our datasets. In each simulation, the magnitudes thus generated are analyzed in exactly the same way as the real data to obtain m_{2g} and σ_{2g}, and from these (using Eq. A5) an estimate $\tilde{m}_{\mathrm{TRGB}}$. This procedure is then repeated many times in Monte-Carlo fashion, and for the resulting ensemble we calculated the mean $\langle\tilde{m}_{\mathrm{TRGB}}\rangle$ and dispersion $\sigma_{m,\mathrm{TRGB}}$ of the $\tilde{m}_{\mathrm{TRGB}}$ estimates, as well as the mean $\langle\sigma_{2g}\rangle$ of the σ_{2g}. In the simulations we experimented with the choice of the algorithm parameters b, J, and M. We found that accurate results were obtained with $J = 3$, $M = 2$ and a binsize $b = 0.07$ magnitudes (although it should be pointed out that the results are not sensitive to the precise choice of these parameters). These parameters were therefore adopted for the further analysis. The Savitzky-Golay coefficients for this choice of parameters are $c_j = \bar{c}_j/b^2$, with $\bar{c}_0 = -0.0476$, $\bar{c}_1 = \bar{c}_{-1} = -0.0357$, $\bar{c}_2 = \bar{c}_{-2} = 0$, $\bar{c}_3 = \bar{c}_{-3} = 0.0595$. With these parameters we found that $|\langle\tilde{m}_{\mathrm{TRGB}}\rangle - m_{\mathrm{TRGB}}| < 0.01$ magnitudes, independent of the assumed σ. Hence, the algorithm produces unbiased estimates of m_{TRGB}. The formal error on a determination of m_{TRGB} from real data is obtained as follows: (i) we run simulations with the appropriate numbers of stars, for a range of σ values; (ii) we identify the value of σ that yields a value of $\langle\sigma_{2g}\rangle$ that equals the value of σ_{2g} inferred from the data; (iii) the corresponding value of $\sigma_{m,\mathrm{TRGB}}$ is the formal error that was sought. The errors thus inferred are listed in Table 1; typical values are 0.02–0.05 magnitudes.

A.3. Assessment of systematic errors

The Monte-Carlo simulations provide accurate estimates of the formal errors in the m_{TRGB} determinations due to the combined effects of the finite number of stars and the properties of our adopted algorithm. However, they provide no insight into possible systematic errors. We have performed a number of additional tests to assess the influence of possible sources of systematic errors.

A.3.1. Accuracy of the correction term Δm_{2g}

Our estimates for m_{TRGB} are obtained from Eq. (A5), in which we add to the observed magnitude m_{2g} of the $f''_{\mathrm{obs}}(m)$ peak a correction Δm_{2g} that is derived from a model. Any error in the model will change the correction Δm_{2g}, which in turn yields a systematic error in the derived m_{TRGB}. It is therefore important to understand the accuracy of the model.

There are two main parameters in fitting the model defined by Eqs. (A1)–(A3) to an observed histogram, namely the 'step-size' Δf of the function $f_{\mathrm{int}}(m)$, and the dispersion σ of the convolution kernel $E(m)$. These parameters are highly correlated. If (as compared to the best fit model) Δf is increased, then an appropriate simultaneous increase in σ will yield a predicted profile $f_{\mathrm{obs}}(m)$ that is only slightly altered. From experiments with our Monte-Carlo simulations we conclude that for all $0.18 \leq \Delta f \leq 0.38$ one can still obtain an acceptable fit to the observed J band magnitude histogram. At the lower end of this range we require $\sigma = 0.105$ and at the high end $\sigma = 0.169$, neither of which seems entirely implausible for the J band data. The dashed curves in Fig. A2b show the correction factors $\Delta m_{2g}(\sigma_{2g})$ for these models. These can be compared to the solid curve, which pertains to the model with $\Delta f = 0.25$ shown in Fig. A1. A typical value of σ_{2g} for our data is ~ 0.11. Fig. A2b shows that for this σ_{2g} the systematic error in Δm_{2g} (and hence m_{TRGB}) due to uncertainties in Δf is approximately 0.02 magnitudes.

The correction term $\Delta m_{2g}(\sigma_{2g})$ that we have applied to all our data was derived from LMC data in the J band. This would not be adequate if the shape of $f_{\mathrm{int}}(m)$ differs significantly among the I, J and K_S bands, or among the LMC and the SMC. However, visual inspection of Fig. 3 does not strongly suggest that this is the case: the shape of the observed magnitude histograms near the TRGB is similar in all cases. Quantitative analysis supports this,

and demonstrated that values of $0.18 \leq \Delta f \leq 0.38$ are adequate for all our data.

A.3.2. Incompleteness

In our main sample we have only included stars that were confidently detected in all three photometric bands. Fig. 3 shows that for this sample incompleteness starts to be an issue at brightnesses that are only a few tens of a magnitude fainter than the inferred $m_{\rm TRGB}$. One may wonder whether this could have had a systematic influence on the $m_{\rm TRGB}$ determinations. To assess this we applied our algorithm also to a different (extended) sample consisting of those stars that were detected in the I and J bands (irrespective of whether or not they were detected in K_S), which is complete to much fainter magnitudes than the main sample (heavy dashed curves in Fig. 3). The RMS difference between the $m_{\rm TRGB}$ estimates from the main and the extended sample (for those cases where both are available) was found to be 0.04, which can be attributed entirely to the formal errors in these estimates. We therefore conclude that there is no evidence for systematic errors due to possible incompleteness.

A.3.3. Foreground subtraction

Our method for foreground subtraction (see Section 3.1) is based on an empirical scaling of the magnitude histogram for an offset field. To assess the effect of possible uncertainties in the foreground subtraction we have, as a test, done our analysis also without any foreground subtraction (i.e., using the thin solid curves in the $N(m)$ panels of Fig. 3). Even this very extreme assumption was found to change the inferred $m_{\rm TRGB}$ values only at the level of ~ 0.02, which can be attributed entirely to the formal errors in the estimates. We therefore conclude that there is no evidence for systematic errors due to uncertainties in the foreground subtraction.

A.3.4. Extinction

Extinction enters into our analysis in various ways. For the I, J and K_S data we have performed our analysis on data that were not corrected for extinction. Instead, we apply an average extinction correction to the inferred $m_{\rm TRGB}$ values after the analysis. Obviously, any error in the assumed average extinction for the sample translates directly into an error in $m_{\rm TRGB}$. Table 1 lists for each band the shift in $m_{\rm TRGB}$ that would be introduced by a shift of $+0.05$ in the assumed $E(B-V)$ (a shift of -0.05 in the assumed $E(B-V)$ would produce the opposite shift in $m_{\rm TRGB}$). It should be noted that our analysis does not assume that the extinction is constant over the region of sky under study. If there are variations in extinction then this causes an additional broadening of the convolution kernel $E(m)$ beyond what is predicted by observational errors alone. The width of the convolution kernel is not assumed to be known in our analysis, but is calibrated indirectly through our determination of σ_{2g} (the dispersion of the $f''_{\rm obs}(m)$ peak). Hence, any arbitrary amount of extinction variations within the Clouds will neither invalidate our results, nor increase the formal errors.

In our calculation of the bolometric magnitudes $m_{\rm bol}$ of the individual stars in our sample from the observed J and K_S magnitudes we do correct for extinction. The effect of a change in the assumed $E(B-V)$ affects the inferred $m_{\rm TRGB}$ values in a complicated way, because both the magnitudes and the colors of individual stars are affected. We therefore performed our entire analysis of the $m_{\rm bol}$ histograms for three separate assumed values of $E(B-V)$, namely 0.10, 0.15 and 0.20. From these analyses we conclude that an increase in $E(B-V)$ of $+0.05$ decreases the inferred bolometric $m_{\rm TRGB}$ by -0.03 (a shift of -0.05 in the assumed $E(B-V)$ would produce the opposite shift in $m_{\rm TRGB}$). As for the I, J and K_S data, extinction variations within the Clouds will not invalidate the results or increase the formal errors.

A.4. Comparison to other methods

Most previous authors have searched for the magnitude m_1 of the peak in the first derivative $f'_{\rm obs}$ to estimate the magnitude $m_{\rm TRGB}$ of the TRGB discontinuity. While this is a perfectly good approach, it is important to realize that this by itself does not yield an unbiased estimate of $m_{\rm TRGB}$. This was pointed out previously by Madore & Freedman (1995; see their Fig. 3). However, they were not overly concerned with this, since their aim was to test the limitations on determining $m_{\rm TRGB}$ to better than ± 0.2 mag. As a result, it has not been common practice to estimate the bias intrinsic to m_1 and correct for it (as we have done in the similar case of m_2). On the other hand, it has now become possible to determine m_1 with formal errors of order 0.1 mag or less (e.g., Sakai, Zaritsky & Kennicutt 1999; Nikolaev & Weinberg 2000), so it is now becoming important to make it common practice to correct for systematic biases in m_1.

To estimate quantitatively the size of possible biases in the results of previous authors one must do Monte-Carlo simulations for their exact observational setup and analysis procedure, which is beyond the scope of the present paper. However, as an illustration it is useful to consider the result of Nikolaev & Weinberg (2000), who find from 2MASS data for the LMC that $m_{\rm TRGB}(K_S) = 12.3 \pm 0.1$, which conflicts significantly with our result $m_{\rm TRGB}(K_S) = 11.98 \pm 0.04$ (see Section 4.4). Nikolaev & Weinberg derived their result from an analysis of the derivative of the observed magnitude distribution; the latter is shown as a histogram with 0.2 mag. bins in their Fig. 9. If they used the Sobel edge detection filter suggested by Madore & Freedman (1995) on the histograms that they display, then Monte-Carlo simulations that we have done (similar

to those in Section A.2) indicate that their estimate of m_1 could overestimate $m_{\rm TRGB}$ by as much as $\sim 0.15 \pm 0.06$. If we correct their result for this bias, then we obtain $m_{\rm TRGB}(K_S) = 12.15 \pm 0.12$ for their data, which would be much closer to our result. Romaniello et al. (1999) use a bin size as large as 0.25 mag in their analysis, and their estimate of the TRGB magnitude is therefore likely to be biased upward even more.

Our method differs from that employed by Sakai, Madore & Freedman (1996) in that they employ kernel smoothing and estimate $f'_{\rm obs}$ as a continuous function, while we employ histograms. Sakai et al. quote as an advantage of their technique that it avoids the arbitrary choice of bin size and histogram starting point. While this is true, we have not found any evidence that this makes a significant quantitative difference. Our Monte-Carlo simulations indicate that our results obtained from histograms are unbiased to better than 0.01 mag., and we have found this to be true for all histogram starting points and a large range of reasonable bin sizes. However, we should point out that for this to be the case it is important to apply appropriate corrections for systematic biases (which applies equally to histograms estimates and kernel smoothing estimates).

A final issue worth mentioning is the estimation of the formal error in $m_{\rm TRGB}$. We have done this through Monte-Carlo simulations, which is probably the most robust way to do this. By contrast, Sakai, Zaritsky & Kennicutt (1999) quote as the formal error the FWHM of the observed peak in $f'_{\rm obs}$. It should be noted that this is not actually accurate (it is probably conservative). Recall from Section A.1 that for the simplified case in which $a_1 = a_2 \equiv a$ in Eq. (A3), one has $f'_{\rm obs}(m) = a + \Delta f E(m - m_{\rm TRGB})$. Hence, the dispersion of the peak in $f'_{\rm obs}(m)$ measures the random error in the individual stellar magnitude measurements (plus whatever smoothing was applied to the data). This dispersion is independent of the number of stars in the sample (N), and therefore cannot be a measure of the formal error in $m_{\rm TRGB}$. The true formal error (i.e., the dispersion among the results obtained from different randomly drawn samples) scales with the number of stars as $1/\sqrt{N}$.

References

Blanco V.M., Blanco B.M., McCarthy M.F., 1980, ApJ 242, 938

Blanco V.M., McCarthy M.F., 1990, AJ 100, 674

Chiosi C., Bertelli G., Bressan A., 1992, ARA&A 30, 235

Cioni M.R., Habing H.J., Loup C., 1998, in: The Stellar Content of Local Group Galaxies, IAU Symp. 192, p. 72

Cioni M.R., Loup C., Habing H.J., Fouqué P., et al., 2000a, A&AS accepted

Cioni M.R., Messineo M., Habing H.J., 2000b, in preparation

Epchtein N., De Batz B., Capoani L., et al., 1997, The Messenger 87, 27

Ferraro F.R., Montegriffo P., Origlia L., Fusi Pecci F., 1999, AJ in press [astro-ph/9912265]

Fouqué P., Chevallier L., Cohen M., et al., 2000, A&AS 141, 313

Frogel J.A., Blanco V.M., 1983, ApJ 274, L57

Gallart C., 1998, in: The Stellar Content of Local Group Galaxies, IAU Symp. 192, p. 22

Girardi L., Bressan A., Bertelli G., Chiosi C., 2000, A&AS 141, 371

Glass I.S., 1999, in: The Handbook of Infrared Astronomy, Cambridge University Press

Groenewegen M.A.T., Baas F., Blommaert J.A.D.L., et al., 1999, A&AS 140, 197

Iben I.Jr., 1967, ARA&A 5, 571

Iben I.Jr., Renzini A., 1983, ARA&A 21, 271

Lee M.G., Freedman W.L., Madore B.F., 1993, ApJ 417, 553

Loup C., 2000, in: New Views of the Magellanic Clouds, IAU Symp. 190, p. 328

Loup C., et al., 2000, in preparation

Madore B.F., Freedman W.L., 1995, AJ 109, 1645

Montegriffo P., Ferraro F.R., Origlia L., Fusi Pecci F., 1998, MNRAS 297, 872

Mould J., et al., 2000, ApJ in press [astro-ph/9909260]

Nikolaev S., Weinberg M.D., 2000, ApJ submitted [astro-ph/0003012]

Paczynski B., Acta Astr. 20, 47

Press W.H., Teukolsky S.A., Vetterling W.T., Flannery B.P., 1992, Numerical Recipes (Cambridge: Cambridge University Press)

Rebeirot E., Martin N., Mianes P., et al. 1983, A&AS 51, 277

Reid N., Mould J., Thompson I., 1987, ApJ 323, 433

Romaniello M., Salaris M., Cassisi S, Panagia N., 1999, AJ in press [astro–ph/9910082]

Sakai S., Madore B.F., Freedman W.L., 1996, ApJ 461, 713

Sakai S., Zaritsky D., Kennicutt R.C.Jr., 1999, ApJ in press [astro-ph/9911528]

Salaris M., Cassisi S., 1997, MNRAS 289, 406

Salaris M., Cassisi S., 1998, MNRAS 298, 166

Sandage A.R., 1971, in: Nuclei of Galaxies, ed. D.J.K. O'Connel (Amsterdam: North–Holland), p. 601

Soria R., Mould J.R., Watson A.M., et al., 1996, ApJ 465, 79

Sweigart A.V., Greggio L., Renzini A., 1989, ApJS 69, 911

Sweigart A.V., Greggio L., Renzini A., 1990, ApJ 364, 527

Vassiliadis E., Wood P.R., 1993, ApJ 413, 641

Westerlund B.E., 1997, in: The Magellanic Clouds, Cambridge Astrophysics Series 29

Zaritsky D., Harris J., Thompson I., 1997, AJ 114, 1002

Zaritsky D., 1999 AJ 118, 2824